ACS APPLIED MATERIALS & INTERFACES

Research Article

www.acsami.org

Applications of in Situ Raman Spectroscopy for Identifying Nickel Hydroxide Materials and Surface Layers during Chemical Aging

David S. Hall,[†,‡] David J. Lockwood,[§] Shawn Poirier,[§] Christina Bock,[‡] and Barry R. MacDougall*[,†,‡]

[†]Department of Chemistry, University of Ottawa, D'Iorio Hall, 10 Marie Curie, Ottawa, Ontario K1N 6N5, Canada

[‡]Energy, Mining and Environment, National Research Council Canada, M-12, 1200 Montreal Rd, Ottawa, Ontario K1A 0R6, Canada

[§]National Research Council Canada, 1200 Montreal Rd, Ottawa, Ontario K1A 0R6, Canada

ABSTRACT: The applications of in situ vibrational spectroscopy for identifying bulk and surface $Ni(OH)_2$ are discussed. Raman spectra from α- and β-$Ni(OH)_2$ samples immersed in water are generally similar to those collected from comparable dry samples. However, the Raman scattering intensities vary, and dry β-$Ni(OH)_2$ additionally exhibits a surface O–H stretching mode at 3690 cm^{-1}. Using in situ Raman spectroscopy, the spontaneous transformation of α-$Ni(OH)_2$ to β-$Ni(OH)_2$ in room-temperature water was monitored. Such transformations are conventionally performed in high-temperature alkaline media. An intralayer OH-diffusion model is proposed. Internal stresses at the α/β-phase boundary caused shifted peaks, higher order vibrational modes, and a new water peak at 3520 cm^{-1}. We conclude that Raman spectroscopy may be applied to observe $Ni(OH)_2$ materials in situ during chemical and electrochemical treatments. Such measurements provide information on the proportions of α- and β-$Ni(OH)_2$ and their fine structural details with high sensitivity.

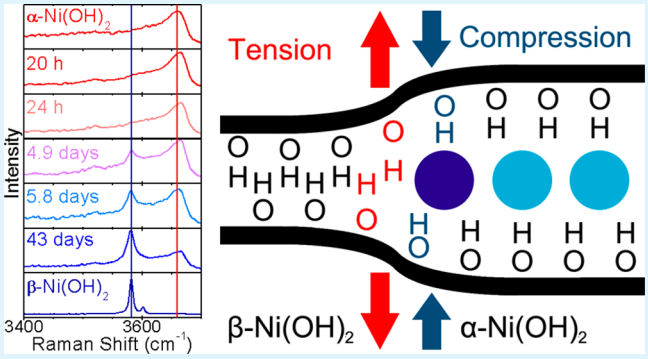

KEYWORDS: *vibrational spectroscopy, Ni(OH)$_2$*

1. INTRODUCTION

$Ni(OH)_2$ materials are important for many potential applications, including energy storage,[1−5] electrochromic devices,[6] and photocatalysis.[7] In the field of corrosion science, $Ni(OH)_2$ components have been observed in electrochemically and air-formed surface layers on Ni metal[8−10] and on many Ni-containing alloys.[11,12]

The fine structural details of $Ni(OH)_2$ materials have direct effects on electrode properties and on device performance. For example, the $Ni(OH)_2$ microstructure affects the electron and proton conductivities and, in turn, the charge-transfer kinetics[13] and the charge capacity[14] of the $Ni(OH)_2$/NiOOH redox pair, which is used extensively for secondary battery anodes (e.g., NiCd and MiMH). In $Ni(OH)_2$-based electrochromic devices, the efficiency and stability during cycling are linked to the Ni(II) salts used during electrode synthesis.[6] Furthermore, the solubility of $Ni(OH)_2$ changes during prolonged storage in solution, which has relevance for chemical-waste management.[15] Lastly, the electrochemical aging of $Ni(OH)_2$ by prolonged voltammetric cycling between Ni(II) and Ni(III) has been shown to improve the kinetics of electrochemical oxygen evolution by up to an order of magnitude.[16] As such, we believe it is worthwhile to consider practical methods to monitor structural changes in $Ni(OH)_2$ materials.

The two phases of $Ni(OH)_2$, denoted α and β, are shown in Figure 1. β-$Ni(OH)_2$ exists naturally as the mineral theophrastite and is isostructural to brucite, $Mg(OH)_2$.[4,17,18] α-$Ni(OH)_2$ consists of planes of β-$Ni(OH)_2$ intercalated with water.[4,19] Although numerous additional phases have been proposed, we recently suggested that there are indeed only two fundamental phases of $Ni(OH)_2$ (α and β). The additional phases can be ascribed to $Ni(OH)_2$ that has adopted various possible structural disorders arising from such factors as impurities, hydration, and crystal defects.[20]

We previously reported how vibrational spectroscopy may be used to evaluate the relative amount of each phase that is present in dry samples rapidly and to determine the types and extents of structural disorder. However, drying $Ni(OH)_2$ samples for analysis introduces stress and can cause physical damage, such as cracking.[20] Hence, this work examines practical considerations for in situ Raman spectroscopy on wet samples. To do this, we measured Raman spectra of pure and mixed α- and β-$Ni(OH)_2$ films that were fully immersed in water immediately after preparation. For comparison, the Raman spectra of comparable dried samples in air were also measured. In the process, we discovered the unexpectedly rapid conversion of α-$Ni(OH)_2$ to β-$Ni(OH)_2$ by measuring the Raman spectra, in situ, during film aging in water at room temperature (22 °C).

Received: August 22, 2013
Accepted: February 6, 2014
Published: February 6, 2014

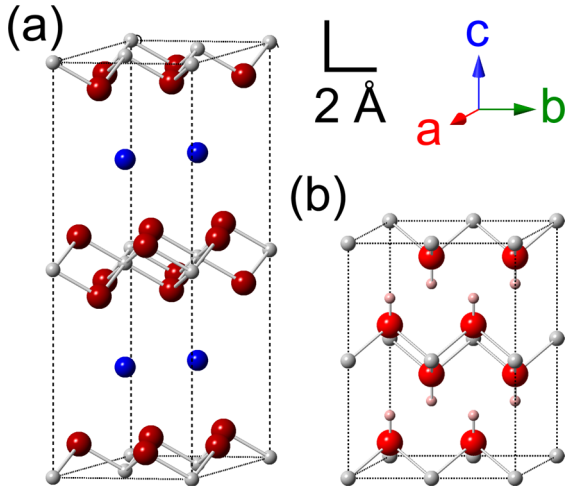

Figure 1. Ball and stick representations of (a) an α-$Ni(OH)_2$ 1 × 1 × 2 supercell and (b) a β-$Ni(OH)_2$ 1 × 2 × 2 supercell: gray, Ni^{2+}; dark red, OH^-; blue, H_2O; red, O^{2-}; and pink, H^+. The structural parameters were adopted from Pandya et al. (α)[21] and Szytula et al. (β).[22] The H^+ positions are unknown for α-$Ni(OH)_2$ because there is no neutron diffraction data available.

2. METHODS

2.1. Material Preparation. Metallic Ni foil (Alfa Aesar, ≥99%, 0.127 mm) electrodes (1 × 2 cm^2) were attached to Ni wire (Alfa Aesar, 99.9%, 0.065 mm diameter) by electric arc welding. The wire and one end of the electrode were covered with Teflon tape. The Ni foil substrates were washed with acetone and ethyl alcohol before they were sonicated in high-purity water (Millipore Milli-Q, 18.2 MΩ cm). Immediately after, the substrates were cleaned in an acid bath (50% v/v acetic acid, 30% phosphoric acid, 10% sulfuric acid, and 10% nitric acid, 85 °C) for 30 s and then rinsed again with excessive amounts of high-purity water.

The α-$Ni(OH)_2$ films were formed by applying −2.5 mA cm^{-2} for 10 min in 0.1 M $Ni(NO_3)_2{\cdot}6H_2O$ (Alfa Aesar, ≥98%). A Ni wire (10 cm long) served as a counter electrode. Electrochemical treatments were performed using a Solartron Analytical 1470E multistat controlled with MultiStat software (v. 1.5a, Scribner Associates Inc.). The solution concentration was selected to allow for efficient precipitation as outlined in previous studies.[20,23] The current density and deposition times were selected to form α-$Ni(OH)_2$ films expected to be sufficiently thick to be identifiable by the spectroscopic methods. The β-phase sample was prepared by aging an α-$Ni(OH)_2$ sample in 30% (w/w) KOH (Fisher Scientific, ACS certified) for 185 h at 90 °C. The β-phase sample was rinsed after aging and stored in water at 22 °C. The sample preparation is very reproducible, as discussed previously.[20]

2.2. Raman Spectroscopy. The Raman measurements were performed at room temperature (22 °C) employing 1 mW of 457 nm laser light (Cobolt Twist diode-pumped solid-state laser) for excitation in a backscattering geometry using the confocal microscope with a 100× objective on a Jobin-Yvon T64000 triple spectrometer operated in the subtractive mode and equipped with a back-illuminated Si charge-coupled-device detector. A relatively short excitation laser wavelength (λ) was employed to increase the experimental intensities. The Raman scattering cross-section is proportional to λ^{-4}. Furthermore, a blue laser is expected to penetrate the films fully, some of which possess a green coloration. Sample measurements were repeated (three spectra were collected for each standard material) to ensure that weak Raman peaks (they usually were also broad peaks) could be positively identified above the background noise level at three locations on the sample. Further details of the measurements have been described previously.[20] The in situ Raman spectra were collected using a 100× immersion lens and the same microscope.

2.3. α-$Ni(OH)_2$ Film Aging. A freshly prepared α-$Ni(OH)_2$ film was thoroughly rinsed and completely immersed in high-purity water at 22 °C. For the Raman measurements, the sample was periodically transferred to a Petri dish filled with high-purity water such that the samples were completely immersed. The sample remained wet at all times to avoid the mechanical strain and cracking that occurs when such films dry.[20] Each measurement was repeated to ensure that Raman peaks were consistent at two locations on the sample. Immediately following each analysis, the sample was returned to the original aging container filled with water.

3. RESULTS AND DISCUSSION

3.1. Raman Spectroscopy of $Ni(OH)_2$ Films Immersed in Water. The Raman spectra of the $Ni(OH)_2$ films, as measured in water, show the expected background water components resulting from backscattering from the laser beam as it traverses the water between the lens and the sample. The spectra also contain fluorescence components, which appear as

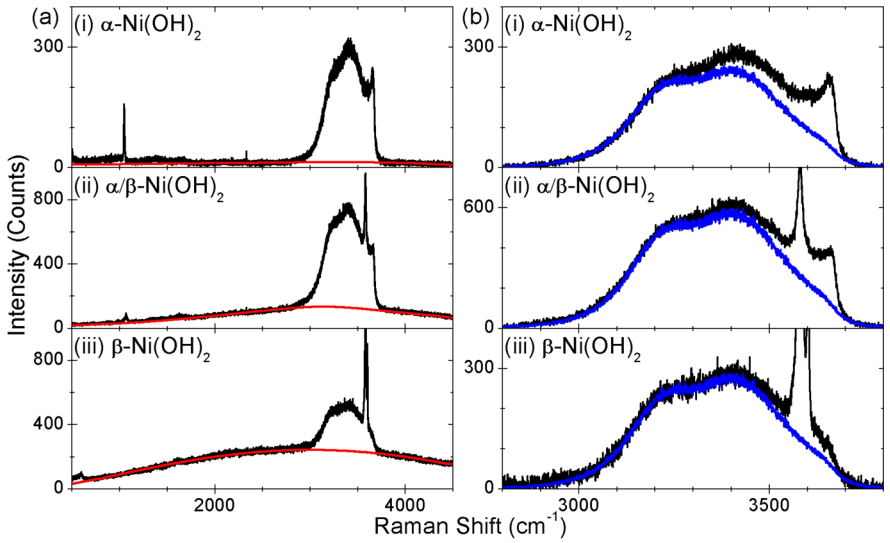

Figure 2. Raman spectra collected from samples immersed in water: (a) the fluorescence background components were first estimated (red) and then subtracted and (b) a reference water spectrum was then rescaled (blue) and subtracted to remove the background water components to reveal features resulting from solely the sample under investigation. Figure 3 shows the resulting spectra.

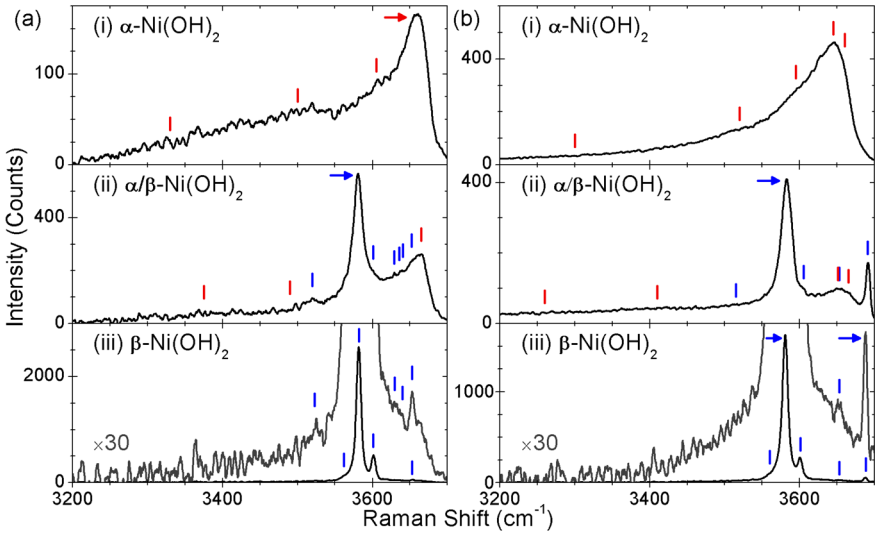

Figure 3. Raman spectra were collected from (a) wet samples immersed in water and (b) dry samples in air. An α-$Ni(OH)_2$ sample was electroprecipitated, transferred to water, and immediately analyzed (a-i). A duplicate α-$Ni(OH)_2$ sample was prepared, immediately dried in air, and then analyzed for comparison (b-i). A mixed-phase sample was prepared by aging α-$Ni(OH)_2$ in room-temperature water and was analyzed while still wet (a-ii). This sample was subsequently dried in air and then reanalyzed for comparison (b-ii). A β-$Ni(OH)_2$ sample was prepared by aging α-$Ni(OH)_2$ in hot KOH solution. The sample was transferred to water and analyzed while still wet (a-iii). This sample was subsequently dried and then reanalyzed for comparison (b-iii). The spectra were smoothed using a Savitzky–Golay filter. The α- and β-phase components listed in Tables 1 and 2 are identified by red and blue tick marks, respectively. Select spectra are enlarged by a factor of 30 to show additional detail.

Table 1. Peak Frequencies and Widths for the O–H Stretching Modes of the Wet-Sample Spectra Shown in Figure 3a

	α				β				
	$\bar{\nu}$		width	peak assignment	$\bar{\nu}$		width	peak assignment	
	cm^{-1}				cm^{-1}			mode	parity
(i)	~3330		broad	layer H_2O[b]					
	~3500		broad	layer H_2O[b]					
	3605	sh[a]	medium	lattice OH					
	3659		medium	lattice OH					
(ii)	~3375		broad	layer H_2O[b]	3520		sharp	A_{1g} – acoustic	even
	~3490	sh[a]	medium	layer H_2O[b]	3581		sharp	A_{1g}	even
	3665		medium	lattice OH	3601	sh	sharp	disordered	even
					3629		very sharp	A_{2u} (TO)[c]	odd
					3636		very sharp	disordered (TO)[c]	odd
					3640		very sharp	A_{2u} (LO)[c]	odd
					3652	sh	sharp	disordered (LO)	odd
(iii)					3523		sharp	A_{1g} – acoustic[c]	even
					3562	sh[a]	sharp	A_{1g} – acoustic	even
					3582		very sharp	A_{1g}	even
					3601		very sharp	disordered	even
					3630		sharp	A_{2u} (TO)[c]	odd
					3640	sh[a]	sharp	A_{2u} (LO)[c]	odd
					3653		sharp	disordered (LO)	odd

[a]sh, shoulder. [b]The layer H_2O modes comprise broad convolutions of several modes. Furthermore, the reported positions of these bands vary considerably between samples.[20] Therefore, the listed peak frequencies are rather imprecise and are provided as approximate values only. [c]The signal-to-noise ratios of these features are very low. Each reported mode was observed in three spectra collected from different areas of the samples and was identified prior to any data smoothing. Furthermore, the positions of these modes closely agree with literature values.[20] These peaks are therefore included in this table. They were not, however, considered during further analysis of the results on account of their low intensities.

broad background peaks (Figure 2a). The intensity of the fluorescence from β-$Ni(OH)_2$ is greater than it is from α-$Ni(OH)_2$, which is consistent with our previous observations from dry samples.[20] The convolution of the water and sample peaks makes it difficult to interpret the raw data properly as collected. To deconvolute the data, the fluorescence components were estimated using B-spline functions and subtracted from the raw data (Figure 2a). The best results were obtained by working with a frequency range that extends at least several hundred cm^{-1} above and ~1000 cm^{-1} below the water O–H stretching bands. Such fluorescence may occur when there is an electronic transition with lower energy than the excitation laser used. Generally, the laser is absorbed, and the analyte is excited into a high-energy state. Following vibrational relaxation, the analyte emits a photon at the fluorescent wavelength. The fluorescence components observed

dx.doi.org/10.1021/am405419k | ACS Appl. Mater. Interfaces 2014, 6, 3141–3149

Table 2. Peak Frequencies and Widths for the O−H Stretching Modes of the Dry-Sample Spectra Shown in Figure 3b

	α				β				
	$\bar{\upsilon}$		width	peak assignment	$\bar{\upsilon}$		width	peak assignment	
	cm^{-1}				cm^{-1}			mode	parity
(i)	3300	sh[a]	broad	layer H_2O[b]					
	3520	sh[a]	medium	layer H_2O[b]					
	3595	sh[a]	medium	lattice OH					
	3645		medium	lattice OH					
	3660	sh[a]		lattice OH					
(ii)	∼3260		broad	layer H_2O[b]	3515	sh[a]	sharp	A_{1g} − acoustic	even
	∼3410		broad	layer H_2O[b]	3583		sharp	A_{1g}	even
	3651		medium	lattice OH	3605		sharp	disordered	even
	3665	sh[a]	medium	lattice OH	3653		sharp	disordered (LO)	odd
					3691		very sharp	surface	even
(iii)					3560		sharp	A_{1g} − acoustic	even
					3581		very sharp	A_{1g}	even
					3601		very sharp	disordered	even
					3653		sharp	disordered (LO)	odd
					3688		sharp	surface	even

[a]sh, shoulder. [b]The layer H_2O modes comprise broad convolutions of several modes. Furthermore, the reported positions of these bands vary considerably between samples.[20] Therefore, the listed peak frequencies are rather imprecise and are provided as approximate values only.

in our spectra peak at 2900−3200 cm^{-1} in Raman shift, which corresponds to a fluorescence maximum at ∼530 nm. This does not match the known visible absorption bands of β-$Ni(OH)_2$ at ∼670 and ∼385 nm.[7,24] Thus, it is unclear whether the fluorescence from β-$Ni(OH)_2$ is intrinsic to the material or whether it arises from structural disorder. Nevertheless, fluorescent components are consistently present in the Raman spectra of β-$Ni(OH)_2$ materials.[20] It is possible to avoid the fluorescence completely by instead using an excitation laser with a longer wavelength than the known band gap of ∼670 nm (e.g., 785 nm). However, as noted, the Raman scattering intensity is proportional to λ^{-4}. Thus, the use of 785 nm would reduce the Raman signal by a factor of 9 compared with the 457 nm excitation used for this work. Because several of the peaks in this work are near the detection limit, we decided that it was preferable to remove the fluorescence computationally than to reduce the instrument's sensitivity and detection limit by using a far-red or an infrared laser.

After the fluorescent components were removed, the resultant spectra contain the $Ni(OH)_2$ peaks superimposed with the water background components (Figure 2b). We collected a reference water spectrum under the same experimental conditions as the $Ni(OH)_2$ samples. The reference spectrum was then scaled to match the intensities of the background water components in the sample measurements by minimizing the residuals over the frequency range 2900−3150 cm^{-1}. The water components were then subtracted to yield the in situ spectra for the wet $Ni(OH)_2$ films (Figure 3a). The resultant peak positions, widths, and intensities match well our previous assignments for the O−H stretching modes and of α- and β-$Ni(OH)_2$ for dry samples.[20] The wet-sample results are summarized in Table 1.

All of the α- and β-phase $Ni(OH)_2$ crystal Raman modes are now well-established, and the lattice modes at frequencies <500 cm^{-1} have been previously studied in detail.[2,13,14,20,25−30] However, these low-frequency modes are not presented or discussed here for the following reasons. It has previously been demonstrated that several of the lattice modes of α-$Ni(OH)_2$, β-$Ni(OH)_2$, and NiO overlap in mixed-phase samples. Thus, the lattice mode vibrational region can be difficult to interpret correctly when studying such mixed-phase materials, as was done here. Furthermore, the measured Raman intensities of these modes are quite low as compared to the O−H stretching mode peaks, and they are especially so for the case of the very thin surface layers investigated here. In contrast, the well-resolved O−H stretching modes have been recommended previously for characterizing mixed-phase α- and β-$Ni(OH)_2$ samples. Furthermore, the O−H stretching modes generally have a greater Raman scattering intensity,[20] which is of particular importance for in situ measurements on thin films, where the signal-to-noise may be quite low. The objective of the present work is to develop reproducible methods that are applicable for a wide variety of applications, including analyses in the presence of high matrix interference or of very limited quantities of $Ni(OH)_2$. Thus, this work primarily focuses on recording and interpreting the frequency range 3000−3700 cm^{-1}. However, it is noteworthy that future investigations may further test the hypotheses and conclusions presented in this work by examining the lower-frequency Raman modes.

To test the validity of our data-treatment method, we collected Raman spectra from analogous dry samples in air for comparison purposes (Figure 3b). We find that there is good agreement of the Raman peak positions between the in situ measurements of the films immersed in water, after the background components have been removed, and the measurements of the dry films collected in air. The peak intensities, however, vary between the wet and dry samples. These variations are readily observed by comparing the relative intensities of the α- and β-phase components from the mixed-phase sample (Figure 3b-i,b-ii). Furthermore, the spectra also exhibit several subtle differences. In particular, the dry β-$Ni(OH)_2$ sample exhibits an additional mode at 3690 cm^{-1}, which has previously been attributed to a surface feature.[20,25] Bernard et al. proposed that the O−H stretching mode of hydroxide groups at the surface is at higher energy than for groups opposed by adjacent layers.[25] When the sample is wetted, the surface hydroxyl groups are opposed by H_2O (i.e., they become hydrated). This is expected to lower the frequency of this surface O−H stretching mode and to increase the peak width relative to a dry sample. Bernard et al. suggest that the

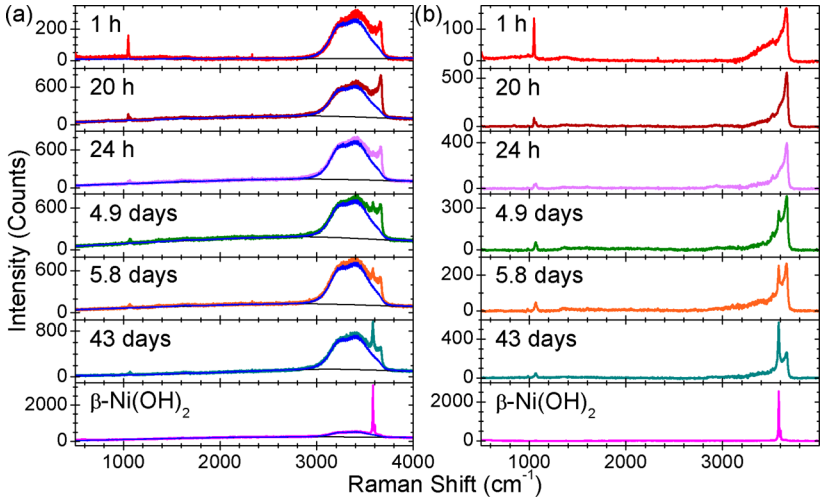

Figure 4. α-Ni(OH)$_2$ film was immersed in room-temperature water immediately after preparation, and Raman spectra were collected periodically, in situ, to monitor the film-aging process. A standard β-Ni(OH)$_2$ film immersed in water was analyzed for comparison. (a) Spectra are shown, as measured, and the fluorescence and background water components were estimated using the method illustrated in Figure 2. (b) Processed spectra are shown after the fluorescence and background water components were removed.

frequency of hydrated surface O−H groups is similar to either the bulk O−H stretching mode (i.e., A_{1g}) or to that of free H_2O.[25] This proposition is consistent with our results, as the peak at 3690 cm^{-1} is completely absent from our measurements of samples immersed in water. Furthermore, this feature is present in both the mixed α/β- and pure β-phase samples, but it is absent in the spectra of the pure α-phase sample. Hence, we conclude that this peak corresponds to dry (i.e., nonhydrated) β-Ni(OH)$_2$ surface hydroxyl groups. The α- and β-phase components observed in the dry-sample Raman spectra are summarized in Table 2.

After removing the fluorescence and background water components, the O−H stretching modes of thin Ni(OH)$_2$ films in water can be readily identified. There is no clear tendency for the absolute peak intensities under the same excitation wavelength (457 nm) and power (1 mW) to be greater for either the wet or dry samples. There are several factors that affect these absolute intensities, including differences in refractive indices between water and air as well as different optical properties of the standard and immersion microscope lenses used for the measurements. Thus, one may consider differences in the Raman scattering intensity for samples measured under the same conditions (i.e., both wet or both dry) but not between the two different experimental setups. Dry β-Ni(OH)$_2$ exhibits an additional surface O−H stretching mode. However, we did not observe any loss in spectral detail by measuring the spectra in situ. There are several weak features included in Tables 1 and 2 that are consistent with literature values for odd-parity or combination transitions of the O−H stretching modes (e.g., the disordered (LO) mode at 3653 cm^{-1}).[20] However, these bands are scarcely above the detection limit of the instrument and are therefore of limited practical value for characterizing such thin films of Ni(OH)$_2$. In contrast, the principle Raman-active O−H stretching modes at ~3660 and 3581 cm^{-1} for α- and β-Ni(OH)$_2$, respectively, have very high Raman scattering intensity. Previously, we have demonstrated that these O−H stretching bands of the lattice OH groups are sufficient for the identification of pure and mixed-phase Ni(OH)$_2$ samples ex situ and that they can provide considerable structural information.[20] Hence, the results of the present work support that Raman spectroscopy has the potential to monitor structural changes during chemical or electrochemical treatments in situ.

3.2. In Situ Raman Spectroscopy of α-Ni(OH)$_2$ Film Aging in Room-Temperature Water. To explore the practical implementation of in situ Raman spectroscopy on Ni(OH)$_2$ materials, we monitored the aging process of α-Ni(OH)$_2$. In alkaline media, α-Ni(OH)$_2$ slowly transforms to β-Ni(OH)$_2$ (1).

$$\alpha\text{-Ni(OH)}_2\cdot\frac{2}{3}\text{H}_2\text{O} \rightarrow \beta\text{-Ni(OH)}_2 + \frac{2}{3}\text{H}_2\text{O} \quad (1)$$

This process is well-studied in alkaline media[4] and in the mother liquor[15] after precipitation of α-Ni(OH)$_2$ by the basification of a Ni(II) salt. Furthermore, the aging process is typically conducted at high temperatures ($T \geq 85$ °C), whereas we monitored the phase transformation in water at room temperature (22 °C). We are only aware of one previous investigation of this process in pure water. However, to collect X-ray diffraction and IR measurements, the researchers periodically removed and dried their samples.[31] It has since been demonstrated that drying such films causes mechanical stress and cracking.[20] Aging may also refer to the transformation of an α-Ni(OH)$_2$ electrode to β-Ni(OH)$_2$ by voltammetric cycling between Ni(OH)$_2$ and NiOOH.[16,29] Our measured spectra, visible in Figure 4a, contain the expected fluorescence and background water components. These were estimated using the methods discussed in the previous section and then removed to produce the spectra shown in Figure 4b.

We previously recommended the use of the O−H stretching modes as a fingerprint region for characterizing α- and β-Ni(OH)$_2$ materials.[20] This region is shown expanded in Figure 5. The characteristic Raman modes for the α (~3660 cm^{-1}) and β (A_{1g}, 3581 cm^{-1}) phases are indicated by vertical black lines on the graph. The phase transformation is easily observed, qualitatively, from the changing relative peak areas of these α- and β-Ni(OH)$_2$ modes. The α-to-β phase transition is quite slow in room-temperature water. At higher temperatures, we

dx.doi.org/10.1021/am405419k | ACS Appl. Mater. Interfaces 2014, 6, 3141−3149

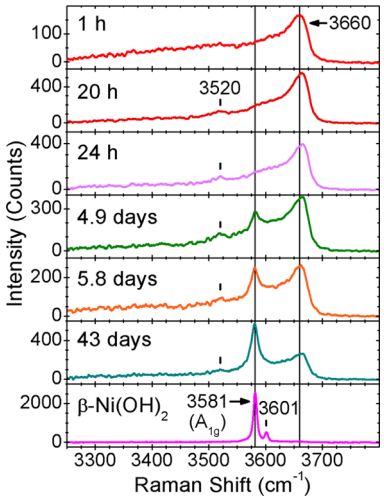

Figure 5. O−H stretching region of the in situ Raman spectra shown in Figure 4b. The characteristic α-Ni(OH)$_2$ (3660 cm^{-1}) and β-Ni(OH)$_2$ (3581 cm^{-1}) O−H stretching modes are indicated by vertical black lines. Two other peaks discussed in the text are denoted by tick marks, and their frequencies are indicated in the figure.

expect that the interlayer water migrates out of the layers more quickly, which results in faster reaction kinetics.

It remains unclear what role, if any, is served by using an alkaline aging solution rather than neutral water. One possibility is that by increasing the ionic strength of the solution the thermodynamic favorability of adding water to the aging solution increases. This is analogous to the effect that electrolyte concentrations have on the osmotic pressures across a membrane. The use of a concentrated electrolyte solution for aging α-Ni(OH)$_2$ may therefore increase the energy difference between the initial and final states. According to transition-state theory, if a decrease in the energy of the final state lowers the reaction rate, then it must be by decreasing the rate of the reverse reaction. Thus, if the addition of an electrolyte to the aging solution indeed increases the dehydration rate, then water moves from the aging solution back into the partially dehydrated material during the aging process. However, further study is necessary to assert this conclusion with confidence. The aging process has been proposed to proceed via dissolution and subsequent reprecipitation in slightly acidic media (pH 4 buffer solution).[32] However, the solubility of Ni(OH)$_2$ in neutral and alkaline media (7 < pH < 14) is very low, which makes a dissolution/precipitation mechanism unlikely for the samples examined in this work.

The β-Ni(OH)$_2$ A$_{1g}$ peak, which appears at 3581 cm^{-1} after 4.9 days, is broader (fwhm ≅ 17 cm^{-1}) than the corresponding peak from the reference material (fwhm ≅ 8 cm^{-1}). Furthermore, the peak maximum is 0.7−1.0 cm^{-1} below the position in the spectrum of the reference material. After 20 h, the α-Ni(OH)$_2$ peak is blue-shifted to ∼3665 cm^{-1}, and a broad feature appears at 3520 cm^{-1}. To explain these observations, we created a simple schematic to represent the essential geometric changes to the crystal structures during the phase transformation (Figure 6). We postulate that the hydroxyl groups near the α/β-phase boundary are subject to compressive and tensile forces, respectively. These stresses are consistent with measured peak shifts and the broadening of the β-Ni(OH)$_2$ A$_{1g}$ peak. We further propose that water molecules near the phase boundary are in a new and chemically distinct environment, which may give rise to the peak at 3520 cm^{-1} and

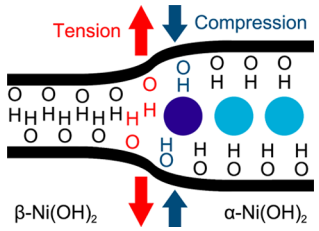

Figure 6. Schematic representation of the α/β-phase boundary during aging. Tensile stress red-shifts the β-Ni(OH)$_2$ O−H stretching mode, and compressive stress blue-shifts the α-Ni(OH)$_2$ O−H stretching mode. Water molecules situated near the phase boundary (dark blue) are expected to have different vibrational frequencies than those in the bulk α-Ni(OH)$_2$ material (light blue).

would be consistent with the disappearance of this peak after the phase transition is complete.

The Raman peak that corresponds to β-Ni(OH)$_2$ stacking fault disorder, at 3601 cm^{-1}, is absent in all of our measurements that were collected during aging. We may therefore conclude that either stacking faults occur at a later stage of the phase transformation or that stacking faults may be avoided by aging samples in room-temperature water.

This work primarily focuses on the O−H stretching modes because of their high Raman scattering intensity relative to the lower-frequency lattice modes. However, it is known that counterions from precursor salts used for precipitation, such as nitrate anions from the Ni(NO$_3$)$_2$ used in this study, are often incorporated into the α-Ni(OH)$_2$ structure during synthesis. Furthermore, nitrate anions incorporated into the α-Ni(OH)$_2$ structure have been observed as intense, prominent features in the vibrational spectra of Ni(OH)$_2$ materials previously.[20,32] After 1 h of aging, we observe a peak at 1049 cm^{-1} (Figure 7),

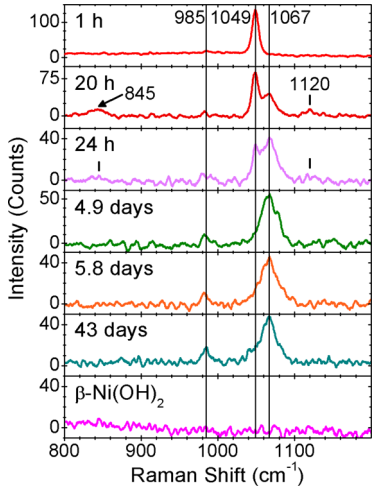

Figure 7. Intermediate frequency range of the in situ Raman spectra shown in Figure 4b. The peaks at 985, 1049, and 1067 cm^{-1} are indicated by vertical black lines. Two other peaks discussed in the text are denoted by tick marks, and their frequencies are indicated in the figure.

which matches the ν_1 stretching mode of free nitrate (i.e., the fully dissociated solution species).[33] At 20 and 24 h, we observe a peak at 845 cm^{-1}, which corresponds with the ν_2 mode of free nitrate,[33] and a weak feature at 1120 cm^{-1}, which we attribute to a combination that involves a nitrate mode. For example, the nitrate ν_4 mode (720 cm^{-1}) and an IR-active lattice mode of α-

dx.doi.org/10.1021/am405419k | ACS Appl. Mater. Interfaces 2014, 6, 3141−3149

$Ni(OH)_2$ (380−400 cm^{-1})[31,34] could yield a Raman-active combination at 1120 cm^{-1}. The emergence of the ν_2 and combination modes indicates that aging introduces structural disorder that relaxes the selection rules.

We previously suggested that nitrate anions sit within the intercalated water planes of the α-$Ni(OH)_2$ structure.[20] In fact, the peak frequencies in the present measurements are closer to those of the free nitrate anion than the spectra that we reported from dry samples. For example, the ν_1 mode of free nitrate is at 1050 cm^{-1}, and we measured a peak at 1049 cm^{-1} from these wet samples, whereas from dry samples, we previously reported a peak at 1047 cm^{-1}.[20,33] Furthermore, the nitrate peaks from dry samples were broader than we observe from our wet samples and than is typical of free nitrate bands. Thus, there is greater similarity between nitrate in the interlayer space and in solution for wet samples than there is for dry samples. This supports a model in which, for dry samples, the interlayer water molecules are frozen in place, whereas for wet samples, the intercalated water has a certain amount of mobility that resembles solution.

We further postulated that nitrate anions may also occupy lattice hydroxyl sites, which corresponded to an additional set of nitrate peaks. These peaks, notably, the intense ν_1 mode at ~997 cm^{-1}, are, however, absent from all of the spectra in the present work, which may indicate that nitrate is quickly (<1 h) expelled from the lattice hydroxyl positions and replaced by hydroxide anions from the interlayer water.

The ν_1 mode intensity decreases considerably over the first 24 h of aging, and no nitrate peaks are visible after 4.9 days. This rapid removal of the nitrate anions indicates a relatively high diffusivity, which further supports the hypothesis that nitrate impurities reside within the loosely defined hydration planes rather than tightly bound lattice sites in the $Ni(OH)_2$ sheets. During the same time period, the intensity of the α-$Ni(OH)_2$ O−H stretching mode more than triples (Figure 5). This indicates that early into the aging process the presence of nitrate anions in the intercalation space creates structural disorder that decreases the O−H stretching mode intensity. For example, one can imagine that the substitution of water molecules with large nitrate anions would warp and deform the $Ni(OH)_2$ sheets along the crystallographic c axis. The high potential energy of this proposed initial state is expected to make the structure relatively unstable and hence may explain the quickness of the nitrate anions' expulsion.

After 20 h, we observe a previously unreported peak at 1067 cm^{-1} (Figure 7). After the peak's initial appearance, its position, intensity, and width are approximately constant over 43 days of aging. Although the peak is close to the ν_1 stretching mode of free carbonate at 1063 cm^{-1},[33] we do not observe any other carbonate modes. Furthermore, the peak is sharper than is typical of combination modes. Hence, we propose that this peak corresponds to a Raman-allowed second-order transition of the E_u (TO) β-$Ni(OH)_2$ mode, which has been reported at 520−550 cm^{-1}.[20] We also observe a peak at 985 cm^{-1}, which we attribute to the second-order transition of the IR-active α-$Ni(OH)_2$ lattice mode at 495 cm^{-1}.[20]

In summary, we applied in situ Raman spectroscopy to monitor the conversion of α-$Ni(OH)_2$ to β-$Ni(OH)_2$ in room-temperature water. The need to dry the samples for analysis was avoided by performing the measurements in situ. The aging reaction was easily monitored using the characteristic O−H stretching modes for α- and β-$Ni(OH)_2$ at 3660 and 3581 cm^{-1}, respectively. The high Raman scattering intensity of these two modes makes them ideal for monitoring chemical and electrochemical processes, even on very thin samples. The dehydration process introduced lattice stress, caused the appearance of higher order lattice modes (985 and 1067 cm^{-1}), blue-shifted the α-$Ni(OH)_2$ O−H stretching mode, and red-shifted and broadened the β-$Ni(OH)_2$ A_{1g} mode. We propose a simple schematic of the phase boundary and consider mechanical forces to explain these observations and to predict a new, intermediate water O−H stretching mode, which we ascribe to a new peak observed at 3520 cm^{-1}. Nitrate anions that were incorporated in the α-$Ni(OH)_2$ structure during electrochemical precipitation were mostly removed after a day, which indicates that they have high diffusivity and supports the hypothesis that nitrate anions sit within the intercalation space.

Although the details of the aging process may be more fully examined by measuring all of the Raman modes, including the less intense, lower-frequency lattice modes, this work demonstrates that considerable information may be practically attained from $Ni(OH)_2$ materials by measuring only the most intense modes. In particular, the identification of the α- and β-$Ni(OH)_2$ components (from the modes at 3660 and 3581 cm^{-1}, respectively), the identification of stacking fault disorder in the β phase (from the mode at 3601 cm^{-1}), the general structural disorder (from O−H stretching mode widths, especially for the β phase), and the incorporation of polyatomic ions (e.g., the intense nitrate ν_1 band at ~1050 cm^{-1}) may be precisely measured in real-time. On account of the high Raman intensity of all of these spectral features, the methods presented in this work may be implemented even for very minute amounts of material or in the presence of very high matrix interference. Future work may extend the application of in situ Raman spectroscopy to $Ni(OH)_2$ materials to include the measurement of ultrathin surface layers (<10^{-7} m) and the less intense lattice modes. Previous work has successfully utilized surface-enhanced Raman spectroscopy (SERS) to measure such ultrathin $Ni(OH)_2$-containing materials and surface layers, including several of the lattice modes.[27−30,35] However, the relative SERS mode intensities are generally difficult to predict and can vary considerably from IR and Raman spectroscopy. Therefore, future spectroscopic investigation utilizing SERS, beyond the scope of the present work, may allow the hypotheses and conclusions presented in this article to be further scrutinized.

4. CONCLUSIONS

In situ Raman spectra were collected and processed from $Ni(OH)_2$ films that were fully immersed in water. The fluorescence and background water spectral features that were also observed can be removed, in that order, using typical spreadsheet or graphical-analysis software. The resultant spectra are similar, but nonidentical, to those obtained from comparable dry samples. Notably, dry β-$Ni(OH)_2$ samples exhibit an additional feature at 3690 cm^{-1} from surface O−H stretching modes. Although the absolute peak intensities vary between wet and dry samples, there was no loss in spectral detail from measuring the samples wet. Thus, Raman spectroscopy is suitable for measuring structural changes in situ during chemical or electrochemical treatments.

Raman spectroscopy was applied to monitor the spontaneous conversion of α-$Ni(OH)_2$ to β-$Ni(OH)_2$ in room-temperature water. By monitoring this aging process in situ, we avoided the physical damage that would have resulted from drying samples for analysis. The transformation from α- to β-$Ni(OH)_2$ was

easily monitored from the relative intensities of the characteristic O−H stretching modes at 3660 and 3581 cm^{-1}, respectively. Nitrate anions that were incorporated in the α-$Ni(OH)_2$ structure during electrochemical precipitation were mostly removed after a day. The dehydration process introduced lattice stress, as evidenced by the appearance of higher-order lattice modes (985 and 1067 cm^{-1}), the blue-shift of the α-$Ni(OH)_2$ O−H stretching mode, and the red-shift and broadening of the β-$Ni(OH)_2$ A_{1g} mode. We propose a schematic of the α/β-phase boundary during aging (Figure 6) and predict a new water O−H stretching mode, which we ascribe to a new peak at 3520 cm^{-1}. Although this aging process is conventionally performed in concentrated alkaline media at high temperature, we observe it also occurs quite simply in room-temperature water. The α-to-β phase transition is quite slow at room temperature, which demonstrates the necessity for elevated temperatures. It remains uncertain what role is served by using an alkaline aging solution, although the presence of an electrolyte may serve to lower the energy of the product.

To date, our work on $Ni(OH)_2$ materials has demonstrated the potential for vibrational spectroscopy to provide information on the proportions of α- and β-$Ni(OH)_2$ and their fine structural details with high sensitivity. FT-IR may be utilized to characterize dry $Ni(OH)_2$ rapidly, whereas Raman spectroscopy offers greater spectral resolution and is well-suited for in situ measurements. Considerable information may be attained from only the most intense Raman modes, making these methods suitable even for very minute amounts of material or in the presence of high matrix interference.

AUTHOR INFORMATION

Corresponding Author

*E-mail: barry.macdougall@nrc.ca. Tel.: 613-991-0914.

Notes

The authors declare no competing financial interest.

ACKNOWLEDGMENTS

This work was supported by National Research Council Canada (NRC) and the Natural Sciences and Engineering Research Council of Canada (NSERC).

ABBREVIATIONS

FT-IR, Fourier-transform infrared
λ, wavelength
$\overline{\upsilon}$, wavenumber
RHE, reversible hydrogen electrode
SERS, surface-enhanced Raman spectroscopy

REFERENCES

(1) Aghazadeh, M.; Golikand, A. N.; Ghaemi, M. Synthesis, Characterization, and Electrochemical Properties of Ultrafine β-$Ni(OH)_2$ Nanoparticles. *Int. J. Hydrogen Energy* **2011**, *36*, 8674−8679.

(2) Gourrier, L.; Deabate, S.; Michel, T.; Paillet, M.; Hermet, P.; Bantignies, J.-L.; Henn, F. Characterization of Unusually Large "Pseudo-Single Crystal" of β-Nickel Hydroxide. *J. Phys. Chem. C* **2011**, *115*, 15067−15074.

(3) Lee, J. W.; Ahn, T.; Soundararajan, D.; Ko, J. M.; Kim, J.-D. Non-Aqueous Approach to the Preparation of Reduced Graphene Oxide/α-$Ni(OH)_2$ Hybrid Composites and Their High Capacitance Behavior. *Chem. Commun.* **2011**, *47*, 6305−6307.

(4) Oliva, P.; Leonarki, J.; Laurent, J. F.; Delmas, C.; Braconnier, J. J.; Figlarz, M.; Fievet, F.; de Guibert, A. Review of the Structure and the Electrochemistry of Nickel Hydroxides and Oxy-Hydroxides. *J. Power Sources* **1982**, *8*, 229−255.

(5) Palacín, M. R. Recent Advances in Rechargeable Battery Materials: A Chemist's Perspective. *Chem. Soc. Rev.* **2009**, *38*, 2565−2575.

(6) Torresi, R. M.; Vázquez, M. V.; Gorenstein, A.; Córdoba de Torresi, S. I. Infrared Characterization of Electrochromic Nickel Hydroxide Prepared by Homogeneous Chemical Precipitation. *Thin Solid Films* **1993**, *229*, 180−186.

(7) Yu, J.; Hai, Y.; Cheng, B. Enhanced Photocatalytic H_2-Production Activity of TiO_2 by $Ni(OH)_2$ Cluster Modification. *J. Phys. Chem. C* **2011**, *115*, 4953−4958.

(8) Hall, D. S.; Bock, C.; MacDougall, B. R. The Electrochemistry of Metallic Nickel: Oxides, Hydroxides, Hydrides and Alkaline Hydrogen Evolution. *J. Electrochem. Soc.* **2013**, *160*, F235−F243.

(9) Medway, S. L.; Lucas, C. A.; Kowal, A.; Nichols, R. J.; Johnson, D. In Situ Studies of the Oxidation of Nickel Electrodes in Alkaline Solution. *J. Electroanal. Chem.* **2006**, *587*, 172−181.

(10) Visscher, W.; Barendrecht, E. Anodic Oxide Films of Nickel in Alkaline Electrolyte. *Surf. Sci.* **1983**, *135*, 436−452.

(11) Machet, A.; Galtayries, A.; Zanna, S.; Klein, L.; Maurice, V.; Jolivet, P.; Foucault, M.; Combrade, P.; Scott, P.; Marcus, P. XPS and STM Study of the Growth and Structure of Passive Films in High Temperature Water on a Nickel-Base Alloy. *Electrochim. Acta* **2004**, *49*, 3957−3964.

(12) Zhang, X.; Zagidulin, D.; Shoesmith, D. W. Characterization of Film Properties on the NiCrMo Alloy C-2000. *Electrochim. Acta* **2013**, *89*, 814−822.

(13) Bantignies, J. L.; Deabate, S.; Righi, A.; Rols, S.; Hermet, P.; Sauvajol, J. L.; Henn, F. New Insight into the Vibrational Behavior of Nickel Hydroxide and Oxyhydroxide Using Inelastic Neutron Scattering, Far/Mid-Infrared and Raman Spectroscopies. *J. Phys. Chem. C* **2008**, *112*, 2193−2201.

(14) Audemer, A.; Delahaye, A.; Farhi, R.; Sac-Epée, N.; Tarascon, J.-M. Electrochemical and Raman Studies of Beta-Type Nickel Hydroxides $Ni_{1-x}Co_x(OH)_2$ Electrode Materials. *J. Electrochem. Soc.* **1997**, *144*, 2614−2620.

(15) Osińska, M.; Stefanowicz, T.; Paukszta, D. Nickel Hydroxide Ageing Time Influence on Its Solubility in Water Acidified with Sulphuric Acid. *J. Hazard. Mater.* **2004**, *112*, 177−182.

(16) Godwin, I. J.; Lyons, M. E. G. Enhanced Oxygen Evolution at Hydrous Nickel Oxide Electrodes via Electrochemical Ageing in Alkaline Solution. *Electrochem. Commun.* **2013**, *32*, 39−42.

(17) Livingstone, A.; Bish, D. On the New Mineral Theophrastite, a Nickel Hydroxide, from Unst, Shetland, Scotland. *Mineral. Mag.* **1982**, *46*, 1−5.

(18) Marcopoulos, T.; Economou, M. Theophrastite, $Ni(OH)_2$, a New Mineral from Northern Greece. *Am. Mineral.* **1981**, *66*, 1020−1021.

(19) Bode, H.; Dehmelt, K.; Witte, J. Zur Kenntnis der Nickelhydroxidelektrode-I. Über das Nickel(II)-Hydroxidhydrat. *Electrochim. Acta* **1966**, *11*, 1079−1087.

(20) Hall, D. S.; Lockwood, D. J.; Poirier, S.; Bock, C.; MacDougall, B. R. Raman and Infrared Spectroscopy of α and β Phases of Thin Nickel Hydroxide Films Electrochemically Formed on Nickel. *J. Phys. Chem. A* **2012**, *116*, 6771−6784.

(21) Pandya, K. I.; O'Grady, W. E.; Corrigan, D. A.; McBreen, J.; Hoffman, R. W. Extended X-ray Absorption Fine Structure Investigations of Nickel Hydroxides. *J. Phys. Chem.* **1990**, *94*, 21−26.

(22) Szytula, A.; Murasik, A.; Balanda, M. Neutron Diffraction Study of $Ni(OH)_2$. *Phys. Status Solidi B* **1971**, *43*, 125−128.

(23) Streinz, C. C.; Hartman, A. P.; Motupally, S.; Weidner, J. W. The Effect of Current and Nickel Nitrate Concentration on the Deposition of Nickel Hydroxide Films. *J. Electrochem. Soc.* **1995**, *142*, 1084−1089.

(24) Ikeda, K.; Vedanand, S. Optical Spectrum of Synthetic Theophrastite, $Ni(OH)_2$. *Neues Jahrb. Mineral., Monatsh.* **1999**, 21−26.

(25) Bernard, M. C.; Cortes, R.; Keddam, M.; Takenouti, H.; Bernard, P.; Senyarich, S. Structural Defects and Electrochemical Reactivity of β-Ni$(OH)_2$. *J. Power Sources* **1996**, *63*, 247−254.
(26) Deabate, S.; Fourgeot, F.; Henn, F. X-ray Diffraction and Micro-Raman Spectroscopy Analysis of New Nickel Hydroxide Obtained by Electrodialysis. *J. Power Sources* **2000**, *87*, 125−136.
(27) Deabate, S.; Fourgeot, F.; Henn, F. Electrochemical Behaviour of the β(II)-Ni(OH)2/β(III)-NiOOH Redox Couple upon Potentiodynamic Cycling Conditions. *Electrochim. Acta* **2006**, *51*, 5430−5437.
(28) Desilvestro, J.; Corrigan, D. A.; Weaver, M. J. Spectroelectrochemistry of Thin Nickel Hydroxide Films on Gold Using Surface-Enhanced Raman Spectroscopy. *J. Phys. Chem.* **1986**, *90*, 6408−6411.
(29) Desilvestro, J.; Corrigan, D. A.; Weaver, M. J. Characterization of Redox States of Nickel Hydroxide Film Electrodes by in Situ Surface Raman Spectroscopy. *J. Electrochem. Soc.* **1988**, *135*, 885−892.
(30) Kostecki, R.; McLarnon, F. Electrochemical and in Situ Raman Spectroscopic Characterization of Nickel Hydroxide Electrodes. *J. Electrochem. Soc.* **1997**, *144*, 485−493.
(31) Le Bihan, S.; Figlarz, M. Croissance de l'Hydroxyde de Nickel $Ni(OH)_2$ à Partir d'un Hydroxyde de Nickel Turbostratique. *J. Cryst. Growth* **1972**, *13/14*, 458−461.
(32) Rajamathi, M.; Kamath, P. V. On the Relationship Between α-Nickel Hydroxide and the Basic Salts of Nickel. *J. Power Sources* **1998**, *70*, 118−121.
(33) Herzberg, G.; Spinks, J. *Molecular Spectra and Molecular Structure: II. Infrared and Raman Spectra of Polyatomic Molecules*, 6th ed.; D. Van Nostrand Company: New York, 1966; Vol. 2.
(34) Faure, C.; Delmas, C.; Fouassier, M. Characterization of a Turbostratic α-Nickel Hydroxide Quantitatively Obtained from an $NiSO_4$ Solution. *J. Power Sources* **1991**, *35*, 279−290.
(35) Melendres, C. A.; Pankuch, M. On the Composition of the Passive Film on Nickel: A Surface-Enhanced Raman Spectroelectrochemical Study. *J. Electroanal. Chem.* **1992**, *333*, 103−113.